PRAMANA
— journal of
physics

Vol. 52, No. 4
April 1999
pp. 421–434

Single and multiple ionization of N_2 molecules by intense light fields of femtosecond duration

S BANERJEE, G RAVINDRA KUMAR and D MATHUR
Tata Institute of Fundamental Research, Homi Bhabha Road, Mumbai 400 005, India
Email: atmol1@spectrum.tifr.res.in

MS received 15 December 1998; revised 11 February 1999

Abstract. We report studies on the multiple ionization of the N_2 molecule using intense, femtosecond laser pulses. We present details of the experimental characterisation of the light pulses and analysis and detection of the ions produced. Precautions to be taken in intense field ionization experiments are discussed. We illustrate the retrieval of information about different aspects of the ionization process (such as, kinetic energies of the fragments produced, dissociation bond lengths and information on the precursors to fragmentation) using coincidence techniques. We report results of the first measurements of the angular distribution of a highly charged fragment, N^{3+}.

Keywords. Intense laser fields; molecules; ionization; time-of-flight; spectrometry

PACS Nos 33.80; 42.62

1. Introduction

Interaction of matter with intense, pulsed laser fields is currently one of the exciting frontiers of laser physics. Recent technological progress in lasers and other instrumentation has enabled the study of single atoms and molecules under intense excitation with the aim of unravelling the new physics that is present under such excitation. The study of atoms has thrown up many new phenomena like above-threshold ionization, high harmonic generation, stabilization against ionization, etc. The study of molecules under intense excitation provides additional richness to the interaction because of the presence of additional time scales of relaxation, possible competition between ionization and dissociation and the orientation of the bond axis with respect to the polarization axis of the light field. Besides, it also provides the possibilities of observing highly charged, possibly transient, molecular fragments.

Earlier work with moderate light intensity levels of $\sim 10^7$–10^{10} Wcm^{-2} in the last two decades has witnessed impressive progress in development of laser-based mass spectrometry techniques, such as resonance ionization mass spectrometry (RIMS) and resonance-enhanced multiphoton ionization (REMPI) [1,2]. The light intensities at which these techniques become very efficient are readily obtained from a wide range of commercially available lasers, covering the entire wavelength region from the infrared to the ultraviolet. Both

RIMS and REMPI are now widely used tools, and they have contributed immensely to successes in both fundamental and applied studies of the structural and dynamical properties of a gamut of atomic and polyatomic systems.

Laser intensities that are considerably higher than those employed in RIMS and REMPI (say, intensities in excess of 10^{12} W cm^{-2}) produce transient electric fields that are comparable in magnitude to intra-molecular coulombic fields. When molecules are irradiated with such high-intensity fields, nonlinear effects begin to dominate field-molecule interactions, and a host of new phenomena become important enough to have significant influence on the dynamics of many molecular processes. Experiments conducted in the course of the last five years or so have shown that nonlinear processes and dynamics which have no analogue in weak-field, or zero-field, situations are responsible for a plethora of new phenomena such as the ejection of further electrons from the molecular core at internuclear separations far from equilibrium (multiple ionization), emission of high energy photons (harmonic generation), above-threshold dissociation, enhanced ionization, and formation of very-high-energy above-threshold ionization electrons. Studies of such intense-field-molecule interaction effects now constitute the mainstream of research in the interaction of intense light fields with matter [3–8].

The use of high-intensity laser fields also distorts molecular potential energy (PE) surfaces, and experimental manifestations of field-distorted, or "dressed", PE curves include various nonlinear phenomena like above-threshold dissociation (attributable to diabatic or adiabatic crossings of PE curves [9]), bond-softening (brought about by suppression of the potential barrier against dissociation in the vicinity of an avoided crossing [10]), and vibrational trapping (which occurs if a deep enough potential well is formed at large internuclear separations as a result of an avoided curve crossing [11]). Consideration of field-induced distortions of PE curves has also opened up the possibility of exercising some selectivity between these three competing processes in experiments which utilize phase control in a two-colour optical field [12–14]. Recently, attempts have also been made in our laboratory to probe the dissociation and ionization dynamics of polyatomic molecules by considering field-induced distortions of molecular electron density distributions [15,16].

Any insight into the dynamics governing field-induced processes in molecules has to account for one major distinctive feature introduced into the dynamics because of interactions involving linearly-polarized light pulses: the spatial alignment of one or more bonds along the direction of the laser polarization vector. It is established that the field associated with linearly-polarized laser light of intensity greater than $\sim 10^{12}$ W cm^{-2} can induce sufficiently strong torques on an initially-randomly oriented ensemble of linear diatomic and triatomic molecules such that dynamic alignment of the internuclear axes occurs. Experimental manifestations of such alignment are the anisotropic angular distributions of fragments ions produced upon subsequent dissociative ionization of such molecules: ion intensities are maximum in the direction of the laser polarization vector and minimum (frequently zero) in the orthogonal direction. The prospects of spatially aligning molecules by means of linearly-polarized, intense light fields is tantalizing and much of the interest in such alignment processes has been generated in the context of pendular-state spectroscopy [17–19] and coherent control of gas-phase reactions [20].

Experimental manifestations of pendular motion in spatially aligned, linear triatomic molecules were reported from our laboratory in studies on linear triatomic molecules [15,16,21,22]. Propensity rules were deduced which govern the spatial alignment of molecules possessing non linear geometries [23,24]. Multiple ionization processes [25],

intense-field ablation of positive and negative cluster ions [26,27] and the first observations of field-induced negative ions [28] have also been the subject of recent reports from our laboratory. All such experiments in our laboratory were conducted using 35 ps long light pulses (of different wavelengths covering the region from 1064 nm to 355 nm) using a high-intensity Nd:YAG and dye laser system capable of yielding focussed light intensities of $\sim 5 \times 10^{14}$ W cm^{-2} [29].

It is the purpose of this paper to report results of a new series of experiments that have been initiated in our laboratory which extend studies on intense-field interactions to much shorter time scales (110 fs) and much higher laser intensities ($\sim 10^{16}$ W cm^{-2}). The enhancement allows access to new domains of non-perturbative physics of molecular systems in external fields. In the following we present a description of the experimental apparatus and methodologies adopted to study some aspects of molecular dynamics; by way of illustration we describe the first experiments we have conducted on the simple diatomic nitrogen molecule.

2. Experimental setup

2.1 Laser system

2.1.1 Hardware configuration: The laser used in the current experiments is a chirped pulse amplification system. Briefly, the system, which is schematically depicted in figure 1, comprises an oscillator, grating pulse-stretcher, regenerative amplifier (RGA), multipass amplifier and a grating pulse-compressor. The oscillator produces 76 MHz pulses in a titanium sapphire (Ti:S) crystal by Kerr lens modelocking. The average modelocked output power is 450 mW at 90 fs with a bandwidth of 20 nm. These pulses are taken to a folded stretcher configuration which temporally stretches the pulse to about 200 ps. The stretched pulse is then coupled into the RGA. The latter is pumped by ~80 mJ of 532 nm radiation from a 6 nanosecond Nd:YAG laser operating at a repetition rate of 10 Hz. A Pockels cell selects pulses from the oscillator pulse train at 10 Hz which get amplified in the RGA from intensity levels of a few nJ per pulse to about 10 mJ after 11 passes in the RGA. The amplified output pulse is switched out by the Pockels cell. Further amplification is achieved by a multipass amplifier system which increases the pulse energy to 80 mJ. The 200 ps chirped pulse is finally compressed to about 100 fs by the grating pulse-compressor. The final output we obtain from our laser system is 50–55 mJ per pulse, with a pulse duration of 100 fs at a repetition rate of 10 Hz. The resulting output power is ~0.5 TW.

The output beam diameter of our laser light is about 14 mm; the light is linearly polarized. The laser pulse has been temporally, spatially and spectrally characterized at the output and also at various intermediate stages. The temporal characteristics of the pulse are measured on a shot-to-shot basis with an autocorrelator. A small fraction of the laser beam is directed into the autocorrelator and split into two parts, using a pellicle beam splitter. The split beams are then recombined by means of mirrors mounted on two arms. One of the mirrors is on a rotating stage while the other can be linearly translated.The beams are recombined after focussing and are spatially overlapped onto a KDP crystal by means of a concave mirror. The autocorrelation signal, which is non-zero only when the two pulses are temporally overlapped, is measured by a photomultiplier. Single-shot pulse duration measurement of the oscillator output at 76 MHz is carried out by rotating one of the arms which

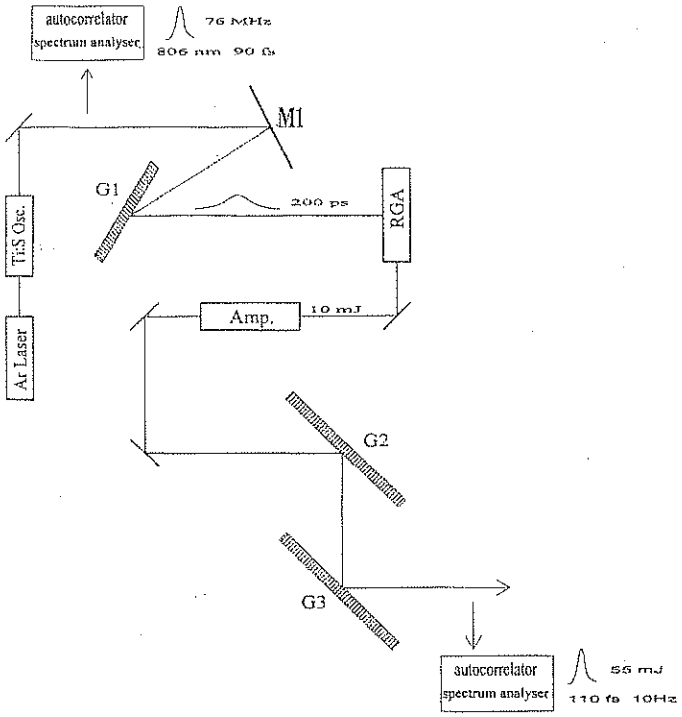

Figure 1. Schematic diagram of the high-intensity femtosecond Ti:S laser system in TIFR's Atomic and Molecular Sciences laboratory. Gratings $G1$ and $M1$ constitute the folded stretch, RGA is the regenerative amplifier, and gratings $G2$, $G3$ constitute the compressor (see text).

provides a variable delay. The temporal pulse profile of the 10 Hz output is measured by providing a linear delay to one of the arms using a stepper-motor-driven translation stage and is a multishot measurement of the pulse duration.

A typical autocorrelation trace for the amplified output is shown in figure 2. A value of 90 fs for the oscillator output is obtained by taking the full width at half maximum (FWHM) of the autocorrelation trace (not shown) after calibration of the rotating delay arm. The pulse duration of the 10 Hz output is calculated by fitting the autocorrelation trace to a Gaussian. The pulse duration of the amplified output was optimized by varying the grating positions in the compressor stage. For these ultrashort pulses the bandwidth is a critical parameter since the temporal width $\Delta\tau$ and the bandwidth $\Delta\nu$ are related by $\Delta\tau\Delta\nu\sim0.55$. The bandwidth and the operating wavelength are monitored using a single shot spectrum analyzer. The inset of figure 2 shows a typical trace. Use of the single-shot spectrum analyzer also enables us to confirm that there is no loss of bandwidth and no modification of the spectral profile in the course of the amplification process in our laser system.

2.1.2 Laser intensity: Ionization of atoms and molecules in light fields is critically

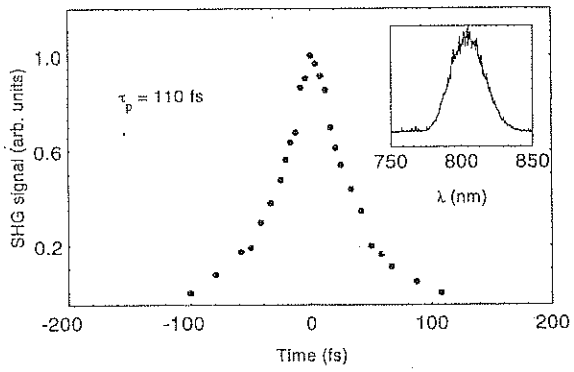

Figure 2. Autocorrelation trace of the amplified output. Inset shows the spectral content of the 110 fs duration pulse.

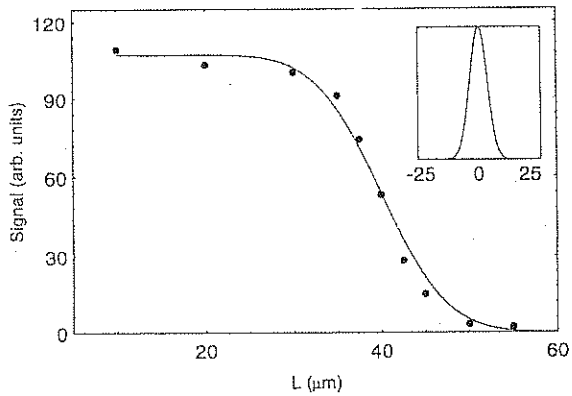

Figure 3. Size of the laser beam at the focus. Circles are experimental points while the solid line is the best fit to the complementary error function. Inset shows the equivalent gaussian.

dependent on the intensity used. To access high intensities in the range of $10^{14} - 10^{16}$ Wcm^{-2} the output laser pulses are focussed by means of a biconvex lens. It is necessary to ascertain the size of the laser spot at the focus in order to have a direct measure of the intensity. There are several ways to accomplish this, e.g. imaging and appearance intensity measurements. In the present series of experiments we have used a scanning knife-edge method which gives a direct measure of the spot size. In this method, a knife-edge is scanned across the beam using a linear translation stage with a resolution of 2.5 μm. The transmitted energy is given by the complementary error function

$$E_T = 1 - E_I \int_x^\infty e^{-(x/b)^2} \mathrm{d}x, \tag{1}$$

where, E_I and E_T are the incident and transmitted energy, respectively, and $2b$ is the spot size of the focussed laser beam. Figure 3 shows a typical trace with an error function

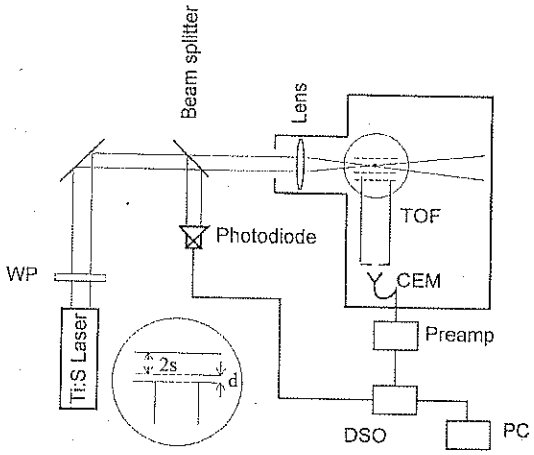

Figure 4. Schematic representation of the experimental setup. Ti:S - high-intensity titanium sapphire laser, WP - waveplate, TOF - linear time-of-flight spectrometer, CEM - channel electron multiplier, Preamp - fast preamplifier, DSO - digital storage oscilloscope, PC - laboratory computer. Circular inset shows the geometry of the laser-molecule interaction zone. Typical ion extraction voltages applied to the plates separated by distance $2s$ are in the range $\pm$10–200 V. The corresponding voltages on the TOF tube are determined by the Wiley–McLaren conditions (see text).

fitting. In order to locate the focussed spot, measurements were made at various positions along the axis in order to obtain not only the size of the focussed spot size but also the Rayleigh range, $\pi\omega^2/\lambda$, that determines the depth of focus. This parameter is of considerable importance, as is discussed in the following. It is to be noted that to avoid damage to the knife edge the input energy had to be kept low ($\sim$nJ) in our measurements. Normand *et al* [30] have shown that it is possible to focus a 1.5 TW beam down to 13.5 μ with a focussed intensity of 10^{18} Wcm^{-2} in vacuum. Since the focussed intensity in our case is 10^{15}Wcm^{-2} under ultrahigh vacuum conditions deviations from the low-intensity values are not expected on account of the negligible effect of nonlinearities.

2.2 Time-of-flight mass spectrometer

Ionization and dissociation of N_2 has been studied using a time-of-flight (TOF) mass spectrometer in a large (85 cm diameter), stainless steel ultra-high-vacuum chamber. Oil-free pumping by means of a 550 ℓs^{-1} turbomolecular pump and getter pump enabled us to routinely obtain background pressures of $\leq 2\times10^{-10}$ mbar. The TOF (figure 4) is a linear two-field instrument where the field E_s accelerates the ions formed in the interaction region and E_d is the ion extraction field. The TOF is operated such that Wiley–McLaren [31] space focussing conditions are satisfied. The distance between the two parallel plates that defines the ion extraction region is 1.5 cm, the acceleration region is 0.5 cm and the TOF drift tube is 22 cm long. Ions are detected using a channel electron multiplier (CEM) operating in the particle counting mode. The CEM output is taken through a fast pulse

preamplifier. The resultant output is recorded using a 500 MHz digital oscilloscope linked to a laboratory computer by a fast data bus.

Our TOF data acquisition scheme is somewhat unusual in that conventional use of time-to-amplitude amplifiers and pulse height analyzers is avoided. The advantage is that the complete TOF spectra can be accumulated on a laser shot-to-shot basis. Subsequent off-line analysis enables reconstruction of either individual "singles" spectra or, as described below, of various coincidence spectra. This facilitates detailed study of ion fragmentation dynamics, including reliable determination of branching ratios for different dissociation pathways.

The high energy femtosecond beam is focussed in the vacuum chamber after passage through a 6 mm thick fused silica-glass window by means of a lens of focal length 10 cm. With the measured focused spot size of 12 μm we deduce a peak laser intensity of 3×10^{15} W cm^{-2} at the focus with an input energy of 5 mJ. Most of the experiments that we report here have been conducted at this intensity. In order to measure TOF spectra at different laser intensities, a set of thin neutral density (ND) filters were used to attenuate the beam by desired factors. It was verified that the temporal pulse profile was not modified by insertion of these ND filters. The polarization state of the laser pulse was controlled by a half-wave plate. The polarization state of the beam after passage through the half-wave plate was calibrated using a thin film polarizer which transmits p-polarization and reflects s-polarization when the laser beam is incident at 72°.

2.3 Data collection, handling and other experimental considerations

Conventional ("singles") mass spectra do not contain any information about the origin of the various fragments which are produced upon dissociative ionization of a molecule. The use of coincidence techniques are necessary in order to probe the dissociation dynamics of N_2^{q+} ($q > 1$) ions produced in the laser-N_2 interaction.

As stated previously, all the ions produced in any given laser shot are collected into our TOF MS; we ensure this by measuring the variation of ion signal as a function of extraction field until saturation of the ion signal is obtained. Once sufficient counts are recorded in every ion channel, which typically requires that mass spectra be recorded for 10000–20000 laser shots, temporal correlations are sought in off-line analysis between different ion-pairs; these correlations are depicted in maps of the type shown below. As in other coincidence measurements, care has to be taken to minimize false coincidences, and the use of the low count rates is mandatory in this respect. In the present experiments we carried out several tests at different gas pressures to ensure that data was acquired under conditions where the effect of false coincidences rate was minimal. For a reliable measure of the temporal correlations between ion pairs in TOF spectra, the ion collection efficiency must approach 100% in order to obtain statistically reliable results. Our measurements were made using ion-extraction voltages that were sufficiently high to ensure large collection efficiency for all ions (see discussion below).

An important facet of the present study is that the data collection methodology to be adopted had to be chosen with extreme care because of opposing constraints placed on experimental conditions by the need to make angle-resolved measurements and coincidence maps. It is known that dissociation of singly-charged molecular ions gives rise to fragments that possess centre-of-mass kinetic energies of, at most, a few hundred meV.

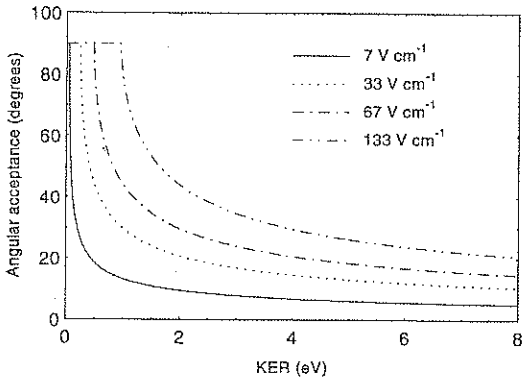

Figure 5. Acceptance angle of the TOF spectrometer for N^+ ions for various values of ion extraction field.

However, dissociation of dication precursors gives rise to fragment-ion kinetic energy release (KER) values that are considerably larger (several eV). The reliability of coincidence measurements using TOF techniques is largely determined by the steps taken to ensure that high-energy fragment ions do not escape detection. Hence, the use of large electrostatic extraction fields in the laser-molecule interaction region is mandatory in TOF configurations. On the other hand, use of large extraction fields leads to reduction of the energy resolution in TOF spectrometers. Furthermore, angular distributions of ions produced upon dissociation of dications may also become distorted by non-uniformities in the extraction field. Indeed, experimental manifestations of pendular motion in angular distribution measurements have hitherto only been obtained with mass filters other than TOF instruments where it is sometimes possible to use zero ion-extraction fields [32,33].

In angular distribution measurements carried out in TOF instruments, the effective angular resolution of the apparatus is essentially determined by the magnitude of the ion extraction field and the KER value associated with each fragment ion. We carried out trajectory simulations through our TOF spectrometer of ions possessing a range of KER values and the results are shown in figure 5 for different values of extraction field. For ions possessing low values of KER, the effective acceptance angle of our TOF spectrometer is large. At low values of ion extraction fields ($\leq$100 V cm^{-1}), fragment ions possessing low KER values ($\sim$500 meV) are detected with an acceptance angle as large as 25° whereas for those with larger KER values ($\sim$3 eV) the corresponding acceptance angle is $\sim$7°. In order to detect high-KER fragments with sufficient efficiency it is clearly necessary to use larger extraction fields. However, this results in degradation of energy resolution. Consequently, we do not present in this report any information on the energy content of the fragments of N_2^{q+} ions. Such data, which has to be obtained in measurements made using low ion extraction voltages, will be presented elsewhere.

Angular distributions of the ions were measured by rotating the polarization direction of the incident laser field with respect to the TOF axis. The polarization direction was rotated in steps of 5°. The shot-to-shot laser intensity was monitored online and measurements were made only for intensity fluctuations which were within $\pm$5%.

Space charge effects [34] also affect the mass spectrum of ions leading to a shift in the position of the peaks and distortion of peak shapes. This arises from primarily three sources: (i) impact ionization of molecules by high energy electrons produced in the focal

volume (ii) scattering of ions by residual gas in the drift tube (iii) electrostatic repulsion between the ions at the point of formation. Ionization by electron impact is negligible if $n\tau F^2 < C$ where n is number density in the interaction region, τ is the pulse duration and F is the field strength. For molecules with ionization potential $\sim$10 eV, the constant $C \sim 10^{23}$. For ultrashort pulses this condition is satisfied for $n < 10^{16}$ cm^{-3} and hence is inconsequential in our case. Scattering in the drift tube is no longer significant if $n < (1/L\sigma_i)$. For a drift length of 22 cm and $\sigma_i \sim 10^{-13}$ we obtain $n \sim 10^{11}$cm^{-3}. The extent of mutual repulsion between ions is a function of the ion density and hence the laser intensity. Thus the working pressure is determined by the latter parameter. Typically at a laser intensity of 10^{15} W cm^{-2} measured flight times of ions are within 1% of calculated ones at a pressure of 10^{-7} torr. At lower intensities $\sim 10^{13}$ W cm^{-2} the working pressure can be as high as 10^{-5} torr without any deleterious effect on the ion flight times. For our case, typical working pressures (with gas load) at an intensity of 2×10^{15}W cm^{-2} were in the range of 6×10^{-9} to 1×10^{-7} torr. These pressures correspond to values of $n = 2\times10^8$–3.5×10^9 cm^{-3}.

3. Results and discussion

3.1 "Singles" TOF spectrum of N_2

Figure 6 shows a typical TOF spectrum of dissociation fragments obtained when N_2 molecules are irradiated with 800 nm light of intensity of 2×10^{15} W cm^{-2}, with a pulse duration of 110 fs. The N_2^+ molecular ion peak (not shown in the TOF spectrum) is much larger than the fragment ion peaks; to put the fragmentation yield in perspective, we note

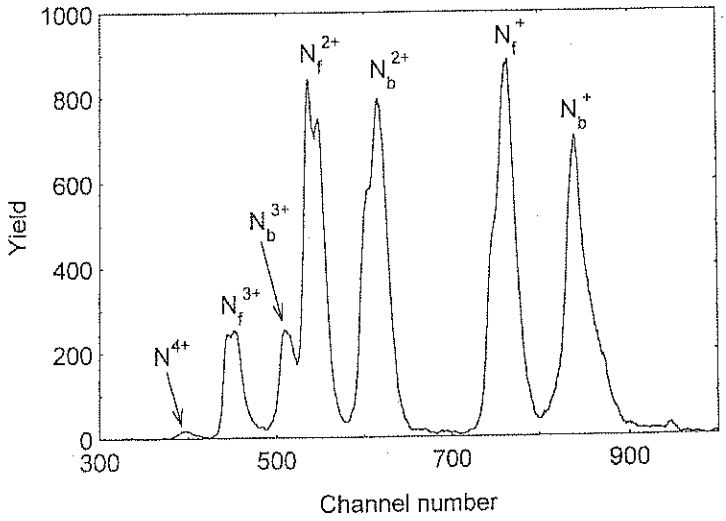

Figure 6. High resolution fragment-ion TOF spectrum of N_2. The subscripts f and b refer to forward and backward directed fragments (see text).

that on the vertical scale of figure 6, the N_2^+ yield was ~7000. Our measurements were made at a working pressure of 8×10^{-9} torr, and the laser's polarization vector was aligned parallel to the axis of the TOF spectrometer. At the pressure used, the mass spectrum is not distorted by space charge effects (see above) [33]. The dynamics of the molecular dissociation and ionization depends on the ionization regime being accessed. The particular regime in which ionization occurs is defined by the Keldysh adiabaticity parameter, γ, which is the ratio of the laser field frequency to the tunneling frequency. Quantitatively,

$$\gamma = \omega(2m_eV_{IE})^{1/2}/eE, \tag{2}$$

where V_{IE} is the zero-field ionization energy of the molecule in its ground state, E is the electric field strength generated by the laser, ω is the angular frequency of the laser field, and e and m_e are the electronic charge and mass, respectively [35]. A value of $\gamma \ll 1$ indicates the tunneling regime while $\gamma \gg 1$ implies multiphoton ionization. Ilkov *et al* [36] have examined this criterion carefully and have suggested a more pragmatic definition of the tunneling regime as γ <0.5. It may be argued that it is unrealistic to expect a single parameter, such as γ, to fully account for the rich dynamics that occur in laser-molecule interactions; taken on their own, the laser wavelength and intensity also play critical roles in the ionization and dissociation process and have to be explicitly considered in discussing the overall dynamics. In the TOF spectrum shown in figure 6, γ=0.14, indicating that our measurements were well in the tunneling regime.

The following features of the TOF spectrum shown in figure 6 are of particular interest in the present study. N^{q+} fragment ions are observed, with $q = 1-4$. Peaks marked f and b represent energetic fragment ions that are ejected in the forward and backward direction, respectively. Their term 'forward' indicates those ions that are formed in a direction that is initially towards the TOF spectrometer; and conversely, 'backward' ions are those that are formed in a direction that is initially away from the TOF spectrometer. The time difference between the f and b ions is a measure of the kinetic energy released upon formation of the ion-pair. The N^{4+} signal was too low for us to be able to distinguish between f and b peaks. The asymmetry of the f and b peaks arises from the fact that backward directed ions have longer flight times as compared to the forward directed ones and hence have a smaller acceptance angle due to the larger displacement in the direction perpendicular to the detector [37].

The different N^{q+} peaks in the TOF spectrum shown in figure 6 clearly indicates that N_2^{q+} ions are formed in charge states higher than 1+. A "singles" spectrum of the type shown in this figure clearly gives no specfic information on the precursor of each ion peak. Coincidence measurements were, therefore, undertaken in order to gain some insight into the nature of the laser-field-induced multiple ionization process in N_2.

3.2 Coincidence measurements

A typical coincidence map obtained at a laser intensity of 2×10^{15} W cm^{-2} is shown in figure 7. The top panel of the figure depicts various ion-pairs that are formed upon unimolecular dissociation of N_2^{q+} ($q \geq 2$) ions. A proper appreciation of the relative branching ratios is obtained by depicting various vertical "slices" through the map. By way of illustration, the lower panel of figure 7 shows the integrated signal obtained when a slice is

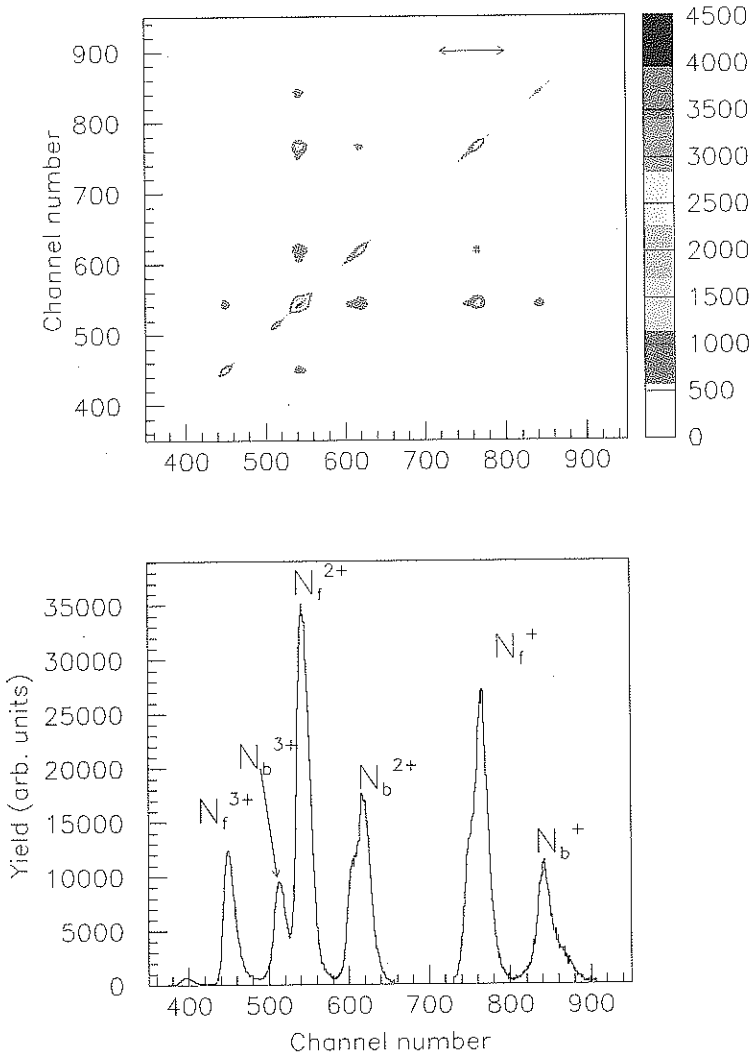

Figure 7. Multi-electron dissociative ionization of N_2 using linearly-polarized light of intensity 6×10^{15} W cm^{-2}. The top panel depicts a coincidence map; the bottom panel shows the integrated ion yield when a slice is taken through the region of the coincidence map that is indicated by the horizontal arrow. The channel numbers are proportional to ion flight time; the channel numbers are proportional to mass/charge ratio of the ions transmitted through the TOF spectrometer. The subscripts f and b indicate forward- and backward-directed fragments (see text).

made through the forward-scattered N_b^+ channel over the range indicated by the horizontal arrow shown on the top panel. The N_b^+–N_b^+ coincidence channel is a reflection of the autocorrelation signal, but all other channels depict real coincidences.

The coincidence measurements also show the assymmetry in the peaks that is observed

in "singles" spectra. Using coincidence data it is possible to unambiguously deduce that the separation between the peaks corresponding to the N^+–N^+ pair is a measure of the most probable KER value upon dissociation of N_2^{2+} dications. Similarly, symmetrical dissociation of N_2^{4+} ions give rise to N^{2+}–N^{2+} ion-pairs. In the case of N_2^{2+}, the most probable KER value is deduced to be 6.7±0.3 eV. The corresponding values obtained for N_2^{4+} and N_2^{6+} are 20.0±2 eV and 35±4 eV, respectively.

Values of KER reflect the internuclear separation (r) at which dissociation of the multiply-charged molecular precursor occurs. The KER distributions can be mapped to the internuclear separation if the potential energy function is known. Using the most probable values of KER in conjunction with Coulombic potentials enables us to deduce that the most probable N–N internuclear distance at which dissociation occurs is the range 2.2–2.5 Å. We note that this analysis is to be regarded as being only semi-quantitative because (i) the entire KER distribution should be mapped into the internuclear separation space and (ii) as shown in earlier work reported from our laboratory, the potential energy functions describing N_2^{q+} ions in high charge states are distinctly non-coulombic [38]. Nevertheless, the present data does serve to indicate that dissociation dynamics proceed with highest probability at internuclear distances larger than equilibrium. Larger than equilibrium bond separations can be used to obtain the associated time scales which we have calculated to be in the range of 10–20 fs.

Enhanced ionization of molecules in short, intense laser pulses at larger than equilibrium internuclear separations, known as critical separations R_c, was initially discovered in theoretical simulations of the ionization rates of H_2^+ [39]; ionization maxima observed in the range of R_c-values 2.5–5.5Å were initially interpreted in terms of electron localization effects brought on by large charge exchange radiative resonance couplings between the highest-occupied and lowest-unoccupied molecular orbitals. Theoretical interpretations of EI in terms of extensions of field-ionization and barrier-suppression ionization models have also been successful [40].

3.3 Angular distributions

We have also used our apparatus to make measurements of the angular distributions of N^{q+} fragment ions. A typical distribution for N^{3+} ions is shown in figure 8. Such measurements were also made at several values of ion extraction voltage; "tighter" angular distributions were obtained as the extraction voltage increased. This has manifested the increase in the angular acceptance angle of the TOF spectrometer with extraction voltage. At very high voltages, the extraction field begins to distort the ion angular distributions, but our calculations (figure 5) show that such values have not been attained in the case of data depicted in figure 8.

The main feature of the morphology of our angular distribution data is clearly the anisotropy. More N^{3+} ions are produced when the laser polarization vector is aligned parallel to the axis of our TOF spectrometer than in the orthogonal direction. This anisotropy reflects the spatial alignment of the precursor molecules in the polarized light field. Experiments are currently underway in our laboratory to exploit the availability of spatially aligned molecules for exploring the new vistas that open up in intense-field molecular dynamics and spectroscopy in the femtosecond domain.

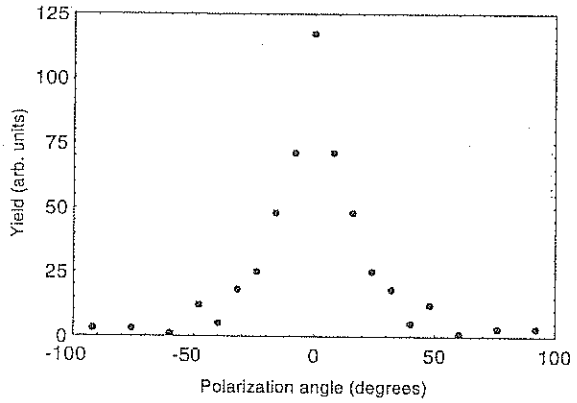

Figure 8. Angular distribution of N^{3+} ions.

Acknowledgements

We thank F A Rajgara for his help in building up the instrumentation for these experiments. We record our appreciation to TIFR for continuing the generous support for the activities of the Atomic and Molecular Sciences laboratory. We are also grateful to the Department of Science and Technology for substantial financial support for our femtosecond laser system.

References

[1] G I Bekov and V S Letokhov, *Appl. Phys.* **B30**, 161 (1983)
[2] G S Hurst and V S Letokhov, *Phys. Today* **47**, 38 (1994)
[3] E Constant, H Stapelfeldt and P B Corkum, *Phys. Rev. Lett.* **76**, 4140 (1996)
[4] A D Bandrauk, *Molecules in Laser Fields*, (Marcel Dekker, New York, 1993)
[5] J L Krause, K J Schafer and K C Kulander, *Phys. Rev. Lett.* **68**, 3535 (1992)
[6] P B Corkum, *Phys. Rev. Lett.* **71**, 1994 (1993)
[7] M Yu Kuchiev, *Phys. Lett.* **A212**, 77 (1996)
[8] A Becker and F H M Faisal, *J. Phys.* **B29**, L197 (1996)
[9] A Giusti-Suzor, F H Mies, L F DiMauro, E Charron and B Yang, *J. Phys.* **B28**, 309 (1995)
[10] P H Bucksbaum, A Zavriyev, H B Muller and D W Schumacher, *Phys. Rev. Lett.* **64**, 1883 (1990)
[11] J E Decker, G Xu and S L Chin, *J. Phys.* **B24**, L281 (1991)
[12] H G Muller, P H Bucksbaum, D W Schumacher, and A Zavriyev, *J. Phys.* **B23**, 2761 (1990)
[13] D W Schumacher, F Wiehe, H G Muller and P H Bucksbaum, *Phys. Rev. Lett.* **73**, 1344 (1994)
[14] B Sheehy, B Walker and L F DiMauro, *Phys. Rev. Lett.* **74**, 4799 (1995)
[15] K Vijayalakshmi, V R Bhardwaj, C P Safvan and D Mathur, *J. Phys.* **B30**, L339 (1997)
[16] K Vijayalakshmi, V R Bhardwaj and D Mathur, *J. Phys.* **B30**, 4065 (1997)
[17] B Friedrich and D Herschbach, *Phys. Rev. Lett.* **74**, 4623 (1995)
[18] G R Kumar, P Gross, C P Safvan, F A Rajgara and D Mathur, *Phys. Rev.* **A53**, 3098 (1996)
[19] G R Kumar, P Gross, C P Safvan, F A Rajgara and D Mathur, *J. Phys.* **B29**, L95 (1996)
[20] E Charron, A Giusti-Suzor and F H Mies, *Phys. Rev.* **A49**, R641 (1994)
[21] G R Kumar, P Gross, C P Safvan, F A Rajgara and D Mathur, *Phys. Rev.* **A53**, 3098 (1996)

[22] D Mathur, V R Bhardwaj, P Gross, G R Kumar, F A Rajgara, C P Safvan and K Vijayalakshmi, *Laser Phys.* **7**, 829 (1997)
[23] V R Bhardwaj, C P Safvan, K Vijayalakshmi and D Mathur, *J. Phys.* **B30**, 3821 (1997)
[24] V R Bhardwaj, K Vijayalakshmi and D Mathur, *Phys. Rev.* **A56**, 2455 (1997)
[25] C P Safvan, F A Rajgara, V R Bhardwaj, G Ravindra Kumar and D Mathur, *J. Phys.* **B29**, 3135 (1996)
[26] C P Safvan, F A Rajgara, V R Bhardwaj, G Ravindra Kumar and D Mathur, *Chem. Phys. Lett.* **255** 25 (1996)
[27] D Mathur, V R Bhardwaj, F A Rajgara and C P Safvan, *Chem. Phys. Lett.* **277**, 558 (1997)
[28] V R Bhardwaj, D Mathur and F A Rajgara, *Phys. Rev. Lett.* **80**, 3220 (1998)
[29] C P Safvan, V R Bhardwaj, G R Kumar, D Mathur and F A Rajgara, *J. Phys.* **B29**, 3135 (1996)
[30] D Normand, M Ferray, L A Lompre, O Gobert, A L'Huillier and G Mainfray, *Optics Lett.* **15**, 1400 (1990)
[31] W C Wiley and I H McLaren, *Rev. Sci. Instrum.* **26**, 1150 (1955)
[32] D Mathur, V R Bhardwaj, P Gross, G R Kumar, F A Rajgara, C P Safvan and K Vijayalakshmi, *Laser Phys.* **7**, 829 (1997)
[33] C P Safvan, R V Thomas and D Mathur, *Chem. Phys. Lett.* **286**, 329 (1998)
[34] M V Ammosov, *Laser Physics* **4**, 431 (1994)
[35] L V Keldysh, *Sov. Phys. JETP* **20**, 1307 (1965)
[36] F A Ilkov, J E Decker and S L Chin, *J. Phys.* **B25**, 4005 (1992)
[37] G R Kumar, V Krishnamurthi and D Mathur, *Rapid Commun. Mass Spectrom.* **7**, 734 (1993)
[38] C P Safvan and D Mathur, *J. Phys.* **B27**, 4073 (1994)
[39] T Zuo, S Chelkowski and A D Bandrauk, *Phys. Rev.* **A48**, 3837 (1993)
[40] T Seideman, M Y Ivanov and P B Corkum, *Phys. Rev. Lett.* **75**, 2819 (1995)